Journal of Ceramic Processing Research. Vol. 17, No. 7, pp. 685~689 (2016)

JOURNAL OF
Ceramic
Processing Research

Crystallite structure, microstructure, dielectric and ferroelectric properties of $BaTi_{0.99}Fe_{0.01}O_{3-\delta}$ ceramic

Han-li Lian*
School of Science, Xi'an University of Posts and Telecommunications, Xi'an, 710121, P.R. China

The $BaTiO_3$ and $BaTi_{0.99}Fe_{0.01}O_{3-\delta}$ ceramics were prepared via a solid state reaction method. The crystallite structure, microstructure, dielectric and ferroelectric properties of the ceramics were studied. The Fe^{3+} ions were soluble into $BaTiO_3$ lattice with the given concentration. The crystallite structure was investigated by using Rietveld refinement and the results show a decrease in the tetragonality due to the doping of Fe^{3+}. Both ceramics have dense microstructures. The mean grain size of $BaTi_{0.99}Fe_{0.01}O_{3-\delta}$ is larger than that of $BaTiO_3$. Compared with $BaTiO_3$, $BaTi_{0.99}Fe_{0.01}O_{3-\delta}$ demonstrates decreased dielectric constant, Curie temperature and ferroelectric properties. A diffuse phase transition behavior was observed on the dielectric constant-temperature curves of $BaTi_{0.99}Fe_{0.01}O_{3-\delta}$. The differences in dielectric and ferroelectric properties between the two ceramics were discussed.

Key words: Ceramic, Crystallite structure, Microstructure, Dielectric properties, Ferroelectric properties.

Introduction

Barium titanate ($BaTiO_3$) is one of classical ferroelectric materials, which has been widely used in electronics industry, such as energy converting systems, multilayer capacitors, sensors with positive temperature coefficient of resistivity, and so on [1-4]. Due to the intrinsic capability of the perovskite structure to host ions with different size, a large number of different dopants can be accommodated in the $BaTiO_3$ lattice. Doping is performed either at the Ba^{2+} and/or Ti^{4+} sites of $BaTiO_3$. Different dopants into $BaTiO_3$ lead to changes in structure and electrical properties [5-6]. $BaTiO_3$-based ceramics with donor dopants (such as Nb^{5+}, La^{3+}) at a relatively low concentration show room-temperature semiconducting character, while the addition of acceptor dopants leads to insulators at room temperature [7-8]. Acceptor dopants of the transition metal ions (such as Ni^{2+}, Fe^{3+}, Co^{3+}, etc) were incorporated into $BaTiO_3$ for the preparation of multilayer ceramic capacitors to allow for the use of cheaper metal electrodes.

Oxygen vacancy is a very significant factor that can affect crystallite structure, microstructure and electrical properties of oxide ceramics. Zhang et al. reported that sintering $(Ba_{0.95}Ca_{0.05})(Ti_{0.88}Zr_{0.12})O_3$ ceramics in a protective atmosphere could increase dielectric constant, which is related to the change in oxygen vacancy concentration [9]. $(K_{0.5}Na_{0.5})NbO_3$ ceramics demonstrate obvious diffuse character of orthorhombic-tetragonal and tetragonal-cubic phase transitions as they have high oxygen vacancy concentration [10]. Jung et al. found that the structural change of grain boundary and related grain growth behavior of $BaTiO_3$ were close related to oxygen partial pressure during sintering [11]. Fujii et al. reported that the moving of domain walls in $BaTiO_3$ was influenced by oxygen vacancy defects [12]. These results show that oxygen vacancy is very important in determining structure and electrical properties of ferroelectric ceramics.

In this work, the $BaTiO_3$ and Fe^{3+}-doped $BaTiO_3$ ceramics were prepared via the solid state reaction method. The crystallite structure, microstructure, dielectric and ferroelectric properties of both ceramics were studied comparatively. The doping of Fe^{3+} into $BaTiO_3$ can induce oxygen vacancies in the ceramic. The changes in structure and electrical properties of the ceramics were discussed according to the effect of oxygen vacancies.

Experimental Methods

The $BaTiO_3$ and $BaTi_{0.99}Fe_{0.01}O_{3-\delta}$ ceramics were prepared via the conventional solid state reaction method. Starting materials are $BaCO_3$ (≥ 99%), TiO_2 (≥ 99%) and Fe_2O_3 (≥ 99%) powders. All raw powders were baked at 100 °C for 24 hrs to remove water and immediately weighed according to the chemical formula. The powders were mixed with zirconia media and ethanol by ball milling for 24 hrs. After drying, the milled powders were calcined at 1000 °C for 2 hrs. The calcined powders were milled again for 12 hrs and then pulverized with approximately 5 wt% polyvinyl alcohol. Pellets of 11.5 mm in diameter and approximately 1.5 mm in thickness were pressed under a uniaxial

*Corresponding author:
Tel : +86-29-88166085
Fax: +86-29-88166085
E-mail: hanlilian@xupt.edu.cn

pressure of 300 MPa and burned out the binder at 500 °C for 2 hrs. The pellets were sintered at 1300 °C for 5 hrs. Heating and cooling rates were 3 °C/min.

Crystallite structure was investigated by means of X-ray diffraction (XRD, Rigaku D/Max 2550) using a Cu K_a radiation. The XRD measurement was made at 40 kV and 100 mA. To obtain the lattice parameters of the ceramics, the XRD patterns were refined via the program of Materials Analysis Using Diffraction (MAUD) [13]. Bulk densities (ρ_b) of the ceramics were measured via the Archimedes method. The theoretical densities (ρ_{th}) were calculated using the following equation:

$$\rho_{th} = M \times Z/(6.02 \times 10^{23} \times V) \quad (1)$$

where *M* is the molar mass of the ceramics, Z is the number of subcell and V is the lattice volume. The relative densities (ρ_r) were obtained via the following formula:

$$\rho_r = \rho_b/\rho_{th} \quad (2)$$

Microstructure of the ceramics was observed using scanning electron microscope (Quanta 200 SEM, FEI Co., Eindhoven, Netherlands). Mean size of grains was determined by means of the linear intercept method.

In order to characterize dielectric and ferroelectric properties of the ceramics, external surfaces of the ceramics were mechanically ground and polished using fine–grained emery paper under cold water circulation. Then, silver electrodes were coated and fired at 650 °C for 30 min. Ferroelectric hysteresis loops were measured at 50 Hz and room temperature in silicon oil with a radiant precision workstation ferroelectric testing system (Radiant Technologies Inc.). Dielectric measurement was performed using an Agilent E4980A precision LCR meter from room temperature to 200 °C at 3 °C/min.

Results and Discussions

XRD curves of $BaTiO_3$ and $BaTi_{0.99}Fe_{0.01}O_{3-\delta}$ are shown in Fig. 1(a, b). Both specimens demonstrate typical ABO_3 perovskite diffraction peaks. No trace of secondary phases was detected within the resolution limit of the apparatus. A magnified view of peaks corresponding to the maximum intensity is shown in Fig. 1(c). It is noted that the XRD peak position of $BaTi_{0.99}Fe_{0.01}O_{3-\delta}$ shifts towards lower diffraction angle direction compared with that of $BaTiO_3$. This can be visualized as an evidence for the dissolution of Fe^{3+} into the lattice structure. According to Shannon's effective ionic radii, Fe^{3+} with a coordination number of six has radius of 0.0645 nm, while Ti^{4+} with a coordination number of six possesses radius of 0.0605 nm [14]. It is known that the substitution site is mainly determined by ionic radius and charge. Though the charge of Fe^{3+} is different from that of Ti^{4+}, the

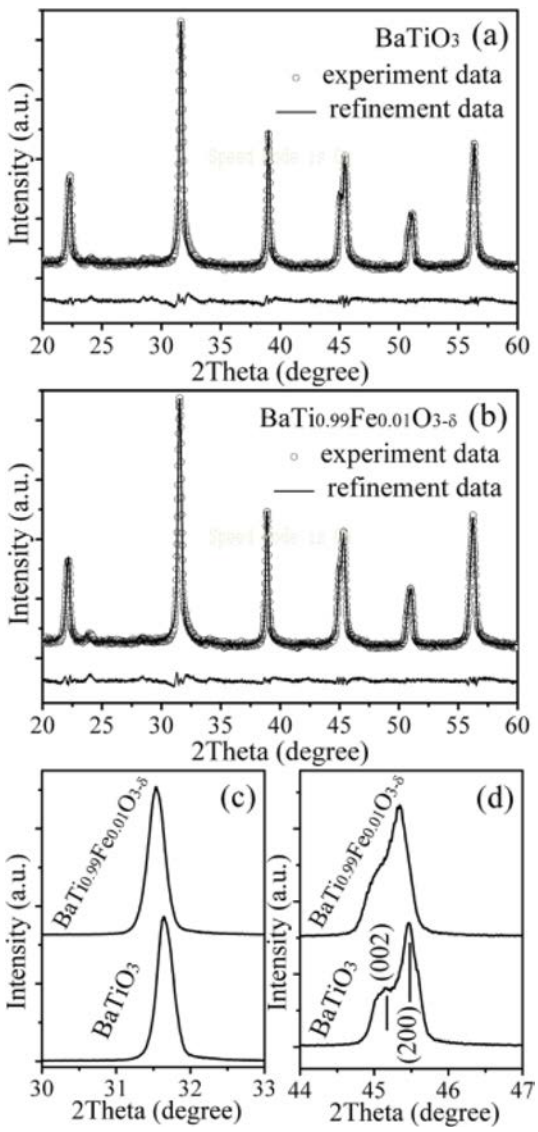

Fig. 1. Rietveld analysis results of XRD pattern for (a) $BaTiO_3$ and (b) $BaTi_{0.99}Fe_{0.01}O_{3-\delta}$. Circles indicate the experiment data and the refinement data are the continuous line overlapping them. The lowest curves in (a) and (b) show the difference between experimental data and refinement data. XRD patterns at 2 theta between 30-33 ° (c) and 44-47 ° (d).

radius of Fe^{3+} is compatible with that of Ti^{4+}. So, Fe^{3+} should substitute Ti^{4+}. With a relatively large size, the incorporation of Fe^{3+} increased the mean radius of the B-site. This led to an increase in the dimension of the unit cells. On the other hand, oxygen vacancies can be formed in $BaTi_{0.99}Fe_{0.01}O_{3-\delta}$ to maintain the overall electrical neutrality according to the Kröger-Vink equation:

$$Fe^{3+} \xrightarrow{BaTiO_3} 2Fe'_{Ti} + V_O^{\bullet\bullet} \quad (3)$$

From the viewpoint of crystal chemistry, the creation of oxygen vacancies can contribute to a decrease in the unit cell dimensions, which should cause a shift of XRD peaks towards higher diffraction angle direction.

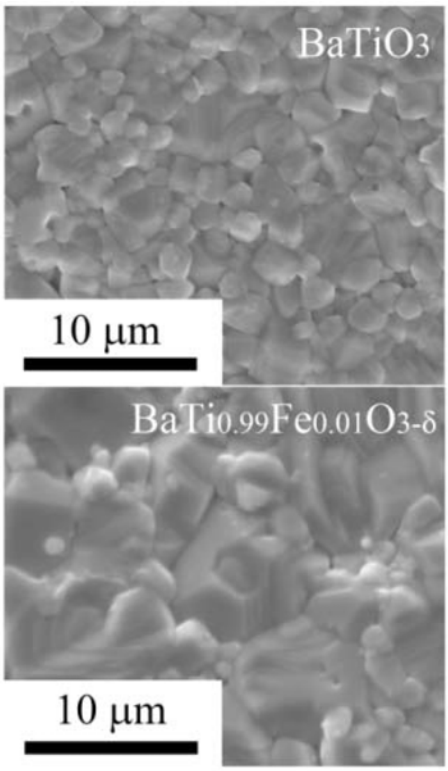

Fig. 2. Typical SEM images of the ceramics.

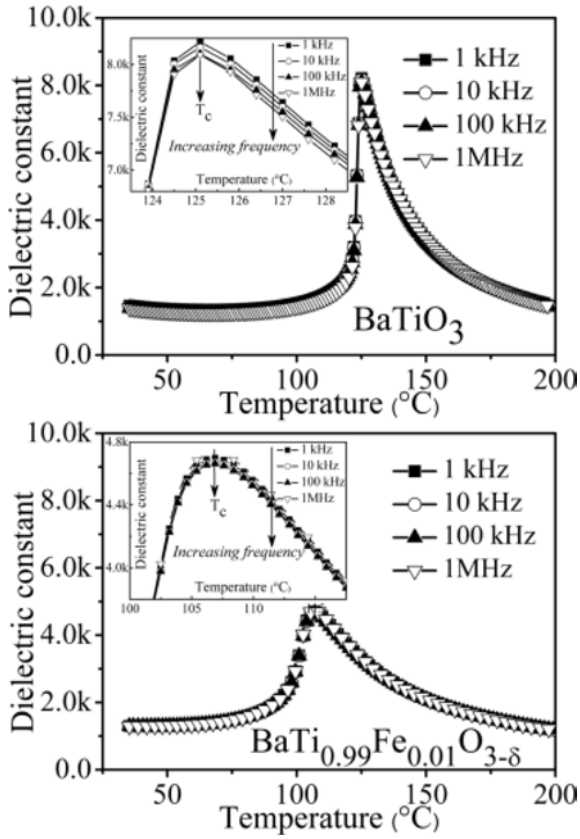

Fig. 3. Plots of dielectric constant vs. temperature for the ceramics. The inserts show the enlarged patterns around the Curie temperatures.

The competition between the two effects is presumed to be responsible for the shift of the XRD peak. Fig. 1(d) shows a magnified view of peaks around $2\theta = 45\,^{o}$. The tetragonal symmetry is always characterized with the presence of (002) and (200) peaks around 45 °. It is found that the splitting of the XRD peaks of $BaTiO_3$ is more obvious than that of $BaTi_{0.99}Fe_{0.01}O_{3-\delta}$, suggesting a decrease in tetragonality for $BaTi_{0.99}Fe_{0.01}O_{3-\delta}$. The lattice parameters of the ceramics were refined by utilizing the program of MAUD with a model of P4mm [13]. After repeated refinement, the values of reliability index parameter (R_{wp}) are less than 15% and the goodness of fit (Sig) has the value between 1.1 ~ 1.3, which confirm the goodness of refinement. The Rietveld analysis results for $BaTiO_3$ and $BaTi_{0.99}Fe_{0.01}O_{3-\delta}$ are demonstrated in Fig. 1(a) and Fig. 1(b), respectively. For $BaTiO_3$, the lattice parameter a is 3.9996 Å and c is 4.0224 Å. The a and c decrease to 4.0021 Å and 4.0199 Å for $BaTi_{0.99}Fe_{0.01}O_{3-\delta}$, respectively. The tetragonality factor c/a-1 decreases from 0.57% for $BaTiO_3$ to 0.44% for $BaTi_{0.99}Fe_{0.01}O_{3-\delta}$.

The bulk densities of $BaTiO_3$ and $BaTi_{0.99}Fe_{0.01}O_{3-\delta}$ are 5.79 and 5.81 g/cm^3, respectively; their relative densities are higher than 95%. SEM images of the ceramics are shown in Fig. 2. Both ceramics show dense microstructure. The mean grain sizes of $BaTiO_3$ and $BaTi_{0.99}Fe_{0.01}O_{3-\delta}$ are about 2.5 and 4.6 μm, respectively. As is generally recognized, the presence of oxygen vacancies in oxide materials is beneficial to mass transport during sintering [15]. As mentioned above, oxygen vacancies were created in $BaTi_{0.99}Fe_{0.01}O_{3-\delta}$, which may contribute to the promoted grain growth in $BaTi_{0.99}Fe_{0.01}O_{3-\delta}$.

Variations in dielectric constant (ε_r) of the ceramics as a function of temperature (T) are shown in Fig. 3. For a given frequency, ε_r increases gradually with an increase in T up to the maximum value of dielectric constant (ε_m) and then decreases. The Curie temperature (T_c) corresponding to ferroelectric-paraelectric phase transition can be determined at ε_m. A sharp peak appears at T_c on the $\varepsilon_r \sim T$ curves of $BaTiO_3$, while the peak of $BaTi_{0.99}Fe_{0.01}O_{3-\delta}$ becomes broad. The inserts of Fig. 3 show the enlarged patterns around T_c. It is found that the T_c values do not change with the increase in frequency from 1 kHz to 1 MHz for a given specimen. For $BaTiO_3$, the T_c value is 125 °C and the ε_m values at 1 kHz, 10 kHz, 100 kHz, 1 MHz are 8216, 8165, 8102, 8093, respectively. For $BaTi_{0.99}Fe_{0.01}O_{3-\delta}$, the T_c value is 107 °C and the ε_m values at 1 kHz, 10 kHz, 100 kHz, 1 MHz are 4698, 4675, 4663, 4613, respectively. For both ceramics, the dielectric loss at room temperature is less than 2%. It is found that ε_m decreases with increasing frequency, which has been widely observed in $BaTiO_3$-based ceramics [16]. The ε_m values of $BaTi_{0.99}Fe_{0.01}O_{3-\delta}$ are lower than those of $BaTiO_3$. It is believed that ferroelectric ceramics with higher oxygen vacancy concentration always have higher ε_m values, which is connected to electron relaxation polarization [9, 17]. The doping of Fe^{3+} into $BaTiO_3$

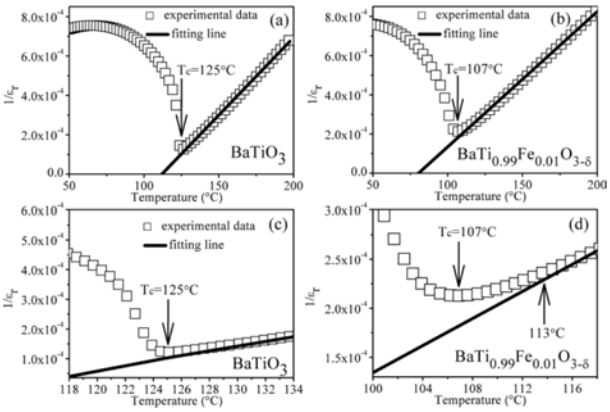

Fig. 4. Plots of the reciprocal of dielectric constant ($1/\varepsilon_r$) at 1 kHz vs. temperature and the fitting plots by the Curie-Weiss law for $BaTiO_3$ (a) and $BaTi_{0.99}Fe_{0.01}O_{3-\delta}$ (b). The corresponding enlarged patterns around the Curie temperatures are shown in (c) and (d). The symbols denote experimental data, while the solid lines denote the least-squared fitting line to the Curie-Weiss law.

caused oxygen vacancies in the ceramic, which facilitates increasing ε_m values. Additionally, the difference in ε_m between $BaTiO_3$ and $BaTi_{0.99}Fe_{0.01}O_{3-\delta}$ is also related to the difference in lattice parameters. It is well known that intrinsic contribution to dielectric constant is from the relative anion/cation shift that preserves the ferroelectric crystal structure. A higher tetragonality always gives higher dielectric constant [18]. So, the decrease in tetragonality factor for $BaTi_{0.99}Fe_{0.01}O_{3-\delta}$ is partially responsible for the reduction of ε_m.

The dielectric properties of the ceramics were studied via Curie-Weiss law;

$$1/\varepsilon_r = (T-T_0)/C \quad (4)$$

where T_0 is Curie-Weiss temperature, and C is Curie constant. Fig. 4 shows the plots of $1/\varepsilon_r$ at 1 kHz vs. T and the fitting plots by the Curie-Weiss law for $BaTiO_3$ and $BaTi_{0.99}Fe_{0.01}O_{3-\delta}$. As shown in Fig. 4(a, c), the data shows a good linear dependence of $1/\varepsilon_r$ vs. $(T-T_0)$ in the paraelectric state above T_c for $BaTiO_3$, suggesting the classical dielectric property of normal ferroelectric materials. It has been reported that the value of $\Delta T = T_c - T_0$ is typically about 8 ~ 15 °C for $BaTiO_3$ [19]. In this work, T_0 is 112 °C and ΔT is 13 °C. The Curie-Weiss plot for $BaTi_{0.99}Fe_{0.01}O_{3-\delta}$ is shown in Fig. 4(b, d). There exists a distinct deviation from Curie-Weiss law below about 113 °C in the paraelectric state. The T_0 is 81 °C and lower than T_c with the value of 26 °C. G.A. Smolenskii pointed out that the order of phase transition can be determined by ΔT, namely $\Delta T = 0$ indicates the ferroelectric-paraelectric phase transition is of a second-order type, while $\Delta T > 0$ is of a first-order transition [20]. Here, the ΔT values for both samples are larger than zero, suggesting a first-order type phase transition.

In order to further characterize the dielectric properties,

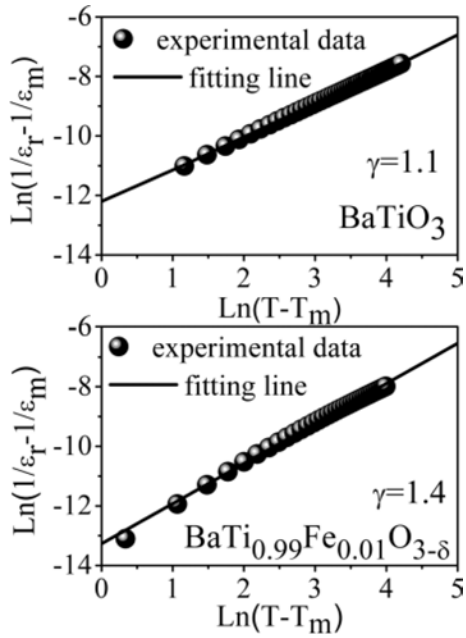

Fig. 5. Plots of $Ln(1/\varepsilon_r - 1/\varepsilon_m)$ vs. $Ln(T-T_c)$ at 1 kHz for $BaTiO_3$ and $BaTi_{0.99}Fe_{0.01}O_{3-\delta}$. The symbols denote experimental data, while the solid lines denote the least-squared fitting line to the modified Curie-Weiss law.

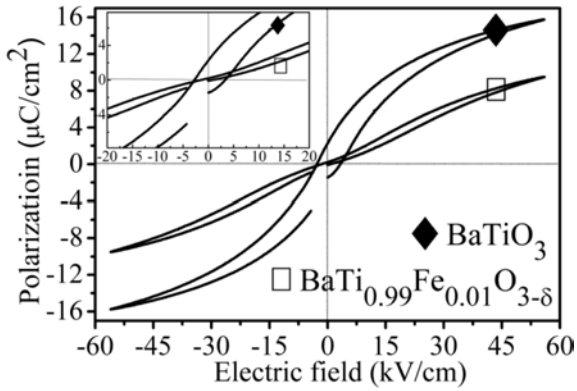

Fig. 6. P-E loops of $BaTiO_3$ and $BaTi_{0.99}Fe_{0.01}O_{3-\delta}$ at 50 Hz and room temperature. The insert shows the enlarged pattern under the electric fields of –20 ~ 20 kV/cm.

a modified Curie-Weiss law was also used [21]:

$$1/\varepsilon_r - 1/\varepsilon_m = (T-T_c)^{\gamma}/C' \quad (5)$$

where ε_m is the maximum value of dielectric constant at the Curie temperature T_c, C' is the Curie-like constant, and g is the degree of diffuseness. g is usually ranging from 1 for a normal ferroelectric to 2 for an ideal relaxor ferroelectric. Plots of $Ln(1/\varepsilon_r - 1/\varepsilon_m)$ as a function of $Ln(T-T_c)$ at 1 kHz for $BaTiO_3$ and $BaTi_{0.99}Fe_{0.01}O_{3-\delta}$ are shown in Fig. 5. Both samples demonstrate a linear relationship. By least-squared fitting the experimental data to the modified Curie-Weiss law, g was determined. The calculated g for $BaTiO_3$ is 1.1, while that for $BaTi_{0.99}Fe_{0.01}O_{3-\delta}$ increases to 1.4. The increase in g implies diffuse character in $BaTi_{0.99}Fe_{0.01}O_{3-\delta}$. The

diffuse phase transition behavior is considered to be close related to the coexistence of complex cations (Fe^{3+} and Ti^{4+}) at an equivalent crystallographic site [22, 23]. Furthermore, the formation of oxygen vacancies in $BaTi_{0.99}Fe_{0.01}O_{3-\delta}$ can increase the local compositional heterogeneity and therefore contributes to more diffusive characteristic of phase transition.

Fig. 6 shows polarization of $BaTiO_3$ and $BaTi_{0.99}Fe_{0.01}O_{3-\delta}$ versus electric field (E_{appl}) measured at 50 Hz and room temperature. Clear hysteresis loop is observed for $BaTiO_3$, which is typical shape for ferroelectric materials. The hysteresis curve of $BaTi_{0.99}Fe_{0.01}O_{3-\delta}$ becomes slim. The hysteresis loops are not completely closed at negative y axis, which is due to the pre-loop delay in the measurement [24]. The remnant polarization (P_r), maximum polarization (P_m) and coercive field (E_c) of the samples were estimated from the hysteresis loops. $BaTiO_3$ shows P_r of 2.25 μC cm^2, P_m of 15.76 μC/cm^2 and E_c of 3.07 kV/cm under E_{appl} = 55 kV/cm. For $BaTi_{0.99}Fe_{0.01}O_{3-\delta}$, the values of P_r, P_m and E_c are 0.21 μC/cm^2, 9.49 μC/cm^2 and 1.45 kV/cm, respectively. The slimmed hysteresis curve causes lower P_r, P_m and E_c values for $BaTi_{0.99}Fe_{0.01}O_{3-\delta}$. The polarization of ferroelectric materials is associated with the distance between the centers of cations and anions in the crystal structure. The coercive field represents the difficulty of domain alignment which is related to the distorted degree of crystal structure and point defects [25, 26]. For the ceramics with tetragonal phase, the distance between the centers of cations and anions in the crystal structure is mainly determined by the lattice constants (a, c). The distorted degree of crystal structure is characterized by the tetragonality factor (c/a-1). The lattice parameter c of $BaTi_{0.99}Fe_{0.01}O_{3-\delta}$ decreases compared with that of $BaTiO_3$. So, a less distorted crystal structure due to the doping of Fe^{3+} into $BaTiO_3$ contributes to a decrease of ferroelectric properties. In addition, Fe^{3+} substituted Ti^{4+} in $BaTi_{0.99}Fe_{0.01}O_{3-\delta}$, which caused an increase in oxygen vacancy concentration. Oxygen vacancies are unfavorable to domain switching, which also led to a decrease in ferroelectric properties [27, 28].

Conclusions

$BaTiO_3$ and $BaTi_{0.99}Fe_{0.01}O_{3-\delta}$ were prepared via the solid state reaction method. Both ceramics show pure perovskite structure with the tetragonal phase. The lattice parameters a and c of $BaTiO_3$ are 3.9996 Å and 4.0224 Å, respectively. For $BaTi_{0.99}Fe_{0.01}O_{3-\delta}$, the a and c decrease to 4.0021 Å and 4.0199 Å, respectively. The doping of Fe^{3+} into $BaTiO_3$ caused a decrease in grain size. Compared with $BaTiO_3$, $BaTi_{0.99}Fe_{0.01}O_{3-\delta}$ shows decreased dielectric constant, decreased Curie temperature, and increased diffuse character. The ferroelectric property of $BaTi_{0.99}Fe_{0.01}O_{3-\delta}$ decreased compared with that of $BaTiO_3$. The change in ferroelectric property was also discussed.

Acknowledgments

This work was supported by the Scientific Research Project of the Education Department of Shaanxi Province, China (No. 15JK1664).

References

1. G. Arlt, D. Hennings, G. de With, J. Appl. Phys. 58 (1985) 1619-1625.
2. G.H. Haertling, J. Am. Ceram. Soc. 82 (1999) 797-818.
3. H. Gong, X. Wang, S. Zhang, H. Wen, L. Li, J. Eur. Ceram. Soc. 34 (2014) 1733-1739.
4. L. Zhang, H. Pan, H. Liu, B. Zhang, L. Jin, M. Zhu, W. Yang, J. Alloys Compds. 643 (2015) 247-252.
5. M.T. Buscaglia, V. Buscaglia, M. Viviani, P. Nanni, M. Hanuskova, J. Eur. Ceram. Soc. 20 (2000) 1997-2007.
6. Y. Ichikawa, Y. Kitanaka, T. Oguchi, Y. Noguchi, M. Miyayama, J. Ceram. Soc. Jap. 122 (2014) 373-380.
7. X. Wang, H.L.-W. Chan, C. Choy, J. Eur. Ceram. Soc. 24 (2004) 1227-1231.
8. Y. Wang, B. Cui, Y. Liu, X. Zhao, Z. Hu, Q. Yan, T. Wu, L. Zhao, Y. Wang, Script Mater. 90-91 (2014) 49-52.
9. S.W. Zhang, H.L. Zhang, B.P. Zhang, G.L. Zhao, J. Eur. Ceram. Soc. 29 (2009) 3235-3242.
10. J.G. Fisher, D. Rout, K.S. Moon, S.J.L. Kang, Mater. Chem. Phys. 120 (2010) 263-271.
11. Y.I. Jung, S.Y. Choi, S.J.L. Kang, Acta Mater. 54 (2006) 2849-2855.
12. I. Fujii, M. Ugorek, Y. Han, S. Trolier-McKinstry, J. Am. Ceram. Soc. 93 (2010) 1081-1088.
13. The MAUD program: http://maud.radiographema.com.
14. R.D. Shannon, Acta Crystallogr. A 32 (1976) 751-767.
15. X.M. Chen, W.Y. Pan, H.H. Tian, X.X. Gong, X.B. Bian, P. Liu, J. Alloys Compds. 509 (2011) 1824-1829.
16. M.E. Lines, A.M. Glass, Principles and applications of ferroelectrics and related materials, Oxford University Press (2001).
17. A. Tkach, P.M. Vilarinho, A.L. Kholkin, Acta Mater. 54 (2006) 5385-5391.
18. J. Rani, K.L. Yadav, S. Prakash, Mater. Sci. Eng. B 178 (2013) 1469-1475.
19. L. Benguigui, Y. Beaucamps, Phys. Rev. B 23 (1981) 5866-5870.
20. G.A. Smolenskii, J. Phys. Soc. Jpn. 28 (1970) 26-37.
21. K. Uchino, S. Nomura, L.E. Cross, S.J. Jang, R.E. Newnham, J. Appl. Phys. 51 (1980) 1142-1145.
22. Q. Xu, D.P. Huang, M. Chen, W. Chen, H.X. Liu, B.-H. Kim, J. Alloy Compd. 471 (2009) 310-316.
23. X.M. Chen, X.X. Gong, T.N. Li, Y. He, P. Liu, J. Alloys Compds. 507 (2010) 535-541.
24. Radiant loop tracer manual: radiant technologies Inc., Application Note, April, 2004.
25. W.C. Lee, Y.F. Lee, M.H. Tseng, C.Y. Huang, Y.C. Wu, J. Am. Ceram. Soc. 92 (2009) 1069-1073.
26. X.M. Chen, H.Y. Ma, W.Y. Pan, M. Pang, P. Liu, J.P. Zhou, Mater. Chem. Phys. 132 (2012) 368-374.
27. T. Friessnegg, S. Aggarwal, R. Ramesh, B. Nielsen, E.H. Poindexter, D.J. Keeble, Appl. Phys. Lett. 77 (2000) 127-129.
28. X.M. Chen, J. Wang, H.Y. Ma, H.L. Lian, P. Liu, J. Ceram. Process Res. 13 (2012) 495-499.